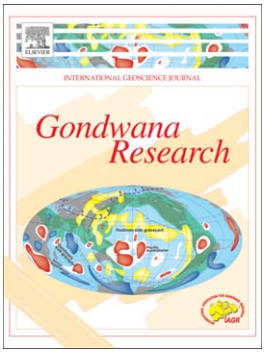

Chemical abrasion applied to SHRIMP zircon geochronology: an example from the Variscan Karkonosze Granite (Sudetes, SW Poland)

Ryszard Kryza, Quentin G. Crowley, Alexander Larionov, Christian Pin, Teresa Oberc-Dziedzic, Ksenia Mochnacka

PII: S1342-937X(11)00199-7
DOI: doi: 10.1016/j.gr.2011.07.007
Reference: GR 674

To appear in: *Gondwana Research*

Received date: 5 February 2011
Revised date: 12 June 2011
Accepted date: 6 July 2011

Please cite this article as: Kryza, Ryszard, Crowley, Quentin G., Larionov, Alexander, Pin, Christian, Oberc-Dziedzic, Teresa, Mochnacka, Ksenia, Chemical abrasion applied to SHRIMP zircon geochronology: an example from the Variscan Karkonosze Granite (Sudetes, SW Poland), *Gondwana Research* (2011), doi: 10.1016/j.gr.2011.07.007

Chemical abrasion applied to SHRIMP zircon geochronology: an example from the Variscan Karkonosze Granite (Sudetes, SW Poland)

Ryszard Kryza [a*], Quentin G. Crowley [b], Alexander Larionov [c], Christian Pin [d], Teresa Oberc-Dziedzic [a], Ksenia Mochnacka [e]

[a] *University of Wrocław, Institute of Geological Sciences, ul. Cybulskiego 30, 50-205 Wrocław, Poland*

[b] *School of Natural Sciences, Department of Geology, Trinity College, Dublin 2, Ireland*

[c] *Centre of Isotopic Research, A.P.Karpinsky All-Russian Geological Research Institute (VSEGEI), 74 Sredny Pr., St. Petersburg, 199 106, Russia*

[d] *Departement de Geologie, CNRS, Universitè Blaise Pascal, 5 rue Kessler, 63038 Clermont-Ferrand, Cedex, France*

[e] *Faculty of Geology, Geophysics and Environmental Protection, Department of Economic Geology, AGH University of Science and Technology, Al. Mickiewicza 30, 30-059 Kraków, Poland*

*Corresponding author. Tel.: +48 71 37 59 371; fax: +48 71 37 59 371.

E-mail address: ryszard.kryza@ing.uni.wroc.pl

E-mail addresses: crowleyq@tcd.ie (Q.G. Crowley), Alexander_Larionov@vsegei.ru (A. Larionov), C.Pin@opgc.univ-bpclermont.fr (C. Pin), teresa.oberc-dziedzic@ing.uni.wroc.pl (T. Oberc-Dziedzic), mochnacka@geol.agh.edu.pl (K. Mochnacka)

Abstract

Thermal annealing followed by acid etching of zircon (chemical abrasion or CA) can be successfully utilised to minimize or eliminate the effects of major and cryptic Pb-loss for SIMS U–Pb zircon dating. The procedure is demonstrated by applying the U–Pb SIMS technique to both untreated and chemically abraded zircons from the Karkonosze Granite, Sudetes, SW Poland. Conventional U–Pb SIMS dating of untreated zircons yields an apparently coherent age population (n=9) with a weighted mean $^{206}Pb/^{238}U$ age of 306±4 Ma. Some untreated zircons display anomalously young $^{206}Pb/^{238}U$ ages (c. 225 and 238 Ma) and are likely to have suffered substantial Pb-loss. A sub-set of zircons from the same sample was chemically abraded. Physically, zircons treated in this manner display a range in the degree of etching and partial dissolution. Extreme examples developed a 3D network of sub-μm channels which follow high-U (dark CL) zones or linear defects, such as micro fractures or indistinct cleavage planes. U–Pb SIMS dating of treated zircons (n=11) yields a mean $^{206}Pb/^{238}U$ age of 322±3 Ma. Two analyses of treated zircons still display younger $^{206}Pb/^{238}U$ ages (c. 297 and 301 Ma) ascribed to the effects of Pb-loss.
For the analysed sample, U–Pb ages determined from chemically abraded zircons are c. 5 % older than those from untreated zircons. This is attributed to effective removal of metamict domains susceptible to Pb-loss. The CA technique also removes micro-inclusions thus lowering common Pb and reducing matrix effects. A cryptic Pb-loss in untreated zircons is only recognised when compared with chemically abraded counterparts or ages determined using other isotope techniques. This clearly demonstrates the utility of CA to high-spatial resolution methods and stresses that Pb-loss is detectable at a range of scales, regardless of the analytical technique used.

Keywords: *Zircon; SHRIMP geochronology; Chemical abrasion; Radiogenic lead loss; Karkonosze Granite*

1. Introduction: problematic Pb-loss in U–Pb geochronology

Modern U–Pb geochronology was developed as a pioneering method in the mid 1950s (Tilton et al., 1955; Wetherill, 1956) and has proven itself to be one of the most robust and widely used for long-lived radiogenic isotope dating. Due to differences in half-lives of parent ^{235}U and ^{238}U isotopes, the technique has routinely been applied to timescale from 800 ka to >4 Ga. Broad age range capability, coupled with a large number of natural mineral chronometers means that the technique has been widely applied in absolute age determination studies. Zircon is by far the most commonly used mineral in U–Pb geochronology. It is formed under variable magmatic and metamorphic conditions, it is very resistant to crustal recycling processes and demonstrates a high closure temperature for Pb (> 900°C; Lee et al., 1997). Despite the positive utilities of the zircon chronometer however, it has long been recognized that the U–Pb isotope system may be disturbed by a process of Pb-loss causing erroneous younger apparent ages. Conditions causing Pb-loss arise from crystal lattice damaged by radiation generating fission tracks, as well as emission of alpha particles and alpha recoil processes (Nasdala et al., 2005). Furthermore, brittle and ductile dislocations may provide pathways for fluid induced Pb-loss. Classically, a careful selection of clear, fractureless grains from a non-magnetic zircon population has been used in order to minimize the effects of such damaged domains and inclusions. Mechanical air-abrasion (Krogh, 1982) has been the method of choice for removing the outermost domains most probably affected by Pb-loss. Conventional dissolution of air-abraded grains followed by ID-TIMS analysis has been the mainstay of high-precision U–Pb geochronology for over two decades. There have been numerous attempts to perfect a method by chemical treatment of zircons to eliminate the effects of Pb-loss. Techniques such as HF etching (Krogh and Davis, 1974, 1975) and partial dissolution (Todt and

Büsch, 1981; McClelland and Mattinson, 1996; Mattinson, 1994) demonstrated varying degrees of success. Thermal annealing of zircons prior to an acid partial digestion (Mundil et al., 2004; Mattinson, 2005; Mattison et al., 2006) proved to be crucial in developing the technique before it became adopted by isotope laboratories worldwide. This was developed exclusively as an effective pre-treatment prior to ID-TIMS analysis. Unlike air-abrasion, "chemical abrasion" (CA) can remove regions of Pb-loss from the interior of grains, even at a very small scale. A few recent studies have demonstrated an improved accuracy when grains are treated by CA producing slightly but significantly older U–Pb ages (e.g. Mundil, 2004). This is presumably due to incomplete removal of areas of Pb-loss from the interior of grains when air-abraded. For the CA technique Mattinson (2005), using a series of incrementally higher temperature partial dissolution steps, demonstrated that at lower temperature leachates showed the highest degree of Pb-loss. At some stage of the partial dissolution process, all portions of zircon which have underwent Pb-loss are removed leaving zircon which is likely to give a concordant analysis and true age.

Whereas Pb-loss has been well documented by ID-TIMS geochronology where multi-grain, whole single grain, or single grain fragments have been analysed, it has less commonly been reported when micro-beam techniques are utilized. This apparent lack of the effects of Pb-loss from micro-beam geochronological data has been heralded as a major advantage of the high degree of spatial resolution inherent in such techniques. Careful selection of apparently pristine domains indeed allows avoidance of potentially damaged parts of grains. Exceptions to this general rule do however exist. For instance, Ashwall et al. (2007) demonstrated that SHRIMP dating of a population of exclusively magmatic, c. 730 Ma old zircon, was subjected to amphibolite facies metamorphism at c. 522 Ma as recorded by growth of metamorphic monazite. The metamorphic event did not result in new zircon growth or resetting of pre-existing magmatic zircon, but caused considerable Pb-loss as documented by both ID-TIMS and SHRIMP dating on the same sample. In a separate U–Pb SHRIMP study of the famous Archaean Jack Hills conglomerate and Mt Narryer

metasediments, Pidgeon and Nemchin (2006) presented data showing extreme Pb-loss which is probably a cumulative effect of events, both in the Archaean and recent times. Pb-loss trajectories are evident from both samples, with some results up to c. 80 % discordant, despite the fact that the authors avoided areas of zircon which were cracked or had visible inclusions or opacity. Whereas such severe Pb-loss is easily recognized, smaller degrees of Pb-loss may yield a result which may still remain concordant, or at least overlaps with the Concordia curve due to the relatively large size of error ellipses (especially on $^{207}Pb/^{235}U$) or degree of Concordia curvature. A Pb-loss identification in such cases is problematic, or even impossible.

Disturbance of mineral chronometers involving radiogenic isotope(s) partial loss is inherent to all isotope systems, whatever analytical technique is used. The unique advantage of the U–Pb system is that it involves two independent, but ideally coupled clocks; this allows to circumvent the negative effects of partial opening provided that the two clocks can be used in combination. Due to relative abundances of radiogenic Pb isotopes however, this results in an intrinsic problem of in situ techniques when applied to recent zircons, because the ^{235}U – ^{207}Pb parent-daughter pair does not give very useful information. In such cases, insufficient ^{207}Pb atoms are available in the micro-volume sputtered or ablated, resulting in poor counting statistics and therefore relatively large analytical uncertainties disguising discordance. Therefore, in situ ages obtained on geological young material are essentially $^{206}Pb/^{238}U$ apparent ages and may be significantly younger than actual formation ages. This is a fundamental constraint; the only way to avoid these problems is to try to eliminate as much as possible the partially opened domains using any sort of abrasion technique.

The objective of this study is to demonstrate that CA can be adapted for micro-beam dating techniques as effectively as it has been documented for ID-TIMS (Mattinson, 2005; Mattison et al., 2006). This is believed to be the first study demonstrating such applicability. We describe a technique which gives greater confidence in ascribing meaningful U–Pb ages to statistically

coherent age populations. We demonstrate by means of comparison of untreated grains from the same sample that recognition of Pb-loss is not necessarily straightforward or obvious even when using micro-beam techniques. Comparison with previously determined Rb-Sr, U–Pb and Ar-Ar ages for the same igneous body supports our interpretation that our CA SIMS data give a meaningful, significantly older magmatic emplacement age for the rock.

The CA test applied by the authors was designed as a provisional attempt to check whether this technique originally designed as a pre-treatment for TIMS analysis (Mattinson, 2005; Mattison et al., 2006) was suited to in-situ dating techniques such as SIMS. Some factors of the analytical protocols, such as the data being collected in two separate analytical sessions and a lower than optimum number of cycle runs, have introduced some additional levels of uncertainty but do not detract from the overall outcome of the experiment. We present a technique which can be applied to any U–Pb SIMS zircon dating where inaccuracy caused by Pb-loss is not a desired result.

2. Geological background of the dated sample

2.1. Geological setting

Large granitic plutons are widespread in the internal part of the central-European Variscides, being a result of intense magmatic activity that culminated between c. 330 and 290 Ma (Kryza et al., 2004; Mazur et al., 2006). One of them, the Karkonosze Granite in the West Sudetes at the northern periphery of the Bohemian Massif, is a c. 60 km long and up to 20 km wide body straddling the Czech/Polish border (Fig. 1). The pluton is located in the core of the Neoproterozoic-Palaeozoic medium-grade metamorphic envelope of the Izera-Karkonosze Massif (Oberc-Dziedzic et al., 2010). The metamorphic envelope of the massif comprises a pile of thrust units, composed

mainly of c. 500 Ma orthogneisses associated with variegated metasedimentary sequences (predominantly mica schists and marbles), and bimodal metavolcanic rocks. The general tectonostratigraphic subdivision of the metamorphic envelope and distribution of the main tectonic units are shown in Figure 1.

The Karkonosze Granite has been intensively investigated, starting with classical granite-tectonic studies by Closs (1925), through detailed geological and petrographic study by Borkowska (1966), Klomínský (1969), Mierzejewski and Oberc-Dziedzic (1990), to more recent petrological research (Ťák and Klomínský, 2007; Słaby and Martin, 2008). Despite being the focus of a comprehensive research, the exact timing of pluton emplacement remains unresolved.

The Karkonosze Pluton comprises several granite types, with two dominating varieties: (a) porphyritic and (b) equigranular (aphyric) granites; other varieties (e.g. "granophyric" type) are subordinate (Borkowska, 1966; Mierzejewski and Oberc-Dziedzic, 1990). Overall, the granite is considered as a late- or post-orogenic pluton (Duthou et al., 1991; Diot et al., 1994; Wilamowski, 1998) of KCG (High-K calk-alkaline granites) type of Barbarin (1999), and of mixed origin (Słaby et al., 2006). Słaby and Martin (2008), based on geochemical modelling, showed that mixing of coeval mantle-derived lamprophyre magmas and crust-derived granitoid magmas strongly influenced the evolution of the predominant porphyritic granites, whereas the equigranular granite facies originated by fractional crystallization.

2.2. Previous geochronology of the Karkonosze Granite

In terms of geochronology, there have been many attempts to date the Karkonosze Granite. The Rb-Sr whole rock isochron method employed by Pin et al. (1987) and Duthou et al. (1991) gave 328±12 Ma for a "central" porphyritic granite and 309±3 Ma for a "ridge" equigranular granite. It is noteworthy that the c. 328 Ma age was obtained both at the scale of the pluton and at the meter

scale, through analysing separately the different layers of a schlieren-bearing block. Pb–Pb evaporation and conventional U–Pb multigrain zircon dating yielded an age of 304±14 Ma for a porphyric monzogranite (Kröner et al., 1994). Subsequent to this, U–Pb SHRIMP zircon ages of 314±3 Ma and 318±4 Ma were determined for porphyritic granites in the NE part of the pluton (Machowiak and Armstrong, 2007), and between 302±6 and 314±5 Ma for other varieties of the granite (Kusiak et al., 2008). $^{40}Ar/^{39}Ar$ dating of a single biotite from a porphyritic Karkonosze Granite ("Liberec-type") gave a plateau age of 320±2 Ma, with the two last high temperature steps at 315 and 314 Ma (Marheine et al., 2002). The eastern part of the Karkonosze Pluton is cut by the Karpacz-Janowice Wielkie dyke swarm, which consists of several tens of mafic (lamprophyric) to felsic dykes cropping out in a NE- -striking zone, c. 20x10 km in size (Awdankiewicz, 2007). Recently, a microgranodiorite dyke of that swarm has been dated using the SHRIMP U–Pb zircon method at 313±3 Ma (average Concordia age for seven points) or 318±3 Ma (selected concordant point), thus approximately constraining the age of the hypabyssal magmatism in the Karkonosze Massif and the minimum age of the host Karkonosze Granite (Awdankiewicz et al., 2010).

Thus, the ages obtained for the Karkonosze Granite so far are scattered between c. 304 and 328 Ma, even for the same granite type. This clearly shows that although fairly precise ages have been obtained (with quoted uncertainties of <1 %), the accuracy of at least some of these results is far from satisfactory. Kusiak et al. (2009) have recently described unusual morphologies and re-equilibration textures in zircons in a Karkonosze Granite sample interpreted as a result of fluid activity at around 304±3 Ma, postdating the emplacement of the main part of the pluton by several millions of years. The zircons in the Karkonosze Granite appear to be U- and Th-rich (see below), thus prone to metamictization and Pb-loss and, consequently, making U-Pb isotopic geochronology difficult.

3. Petrography and sampling

Our sample of porphyritic Karkonosze Granite (SZH) was collected in Szklarska Poręba, from the north side of "Huta" quarry (50.82690N, 15.49446E). Two granite varieties are exposed there: porphyritic granite to the north side, and equigranular granite to the west side of the quarry. Both types are rather inhomogeneous and contain pale-coloured (aplitic) with dark-coloured (biotite-rich) schlieren. The latter are often of banded-type, but some may represent partly diffused enclaves. Both the granite types also bear mafic, fine-grained enclaves of ellipsoid shape and usually 2–5 cm in size. They are tonalitic in composition and contain plagioclase crystals, up to a few millimetres in size, resembling the plagioclase grains in the granite matrix. Plagioclase porphyrocrysts often protrude from the matrix into the enclave. Such enclaves are interpreted as products of incomplete mixing (mingling) of acidic and basic magmas. Both the granites are cut by aplitic veins, up to 20 cm thick, often with small pegmatite nests.

The porphyritic granite studied contains large, up to several cm in size, euhedral porphyrocrysts of pink K-feldspar, often rimmed with whitish plagioclase (rapakivi-type texture), all enclosed in a coarse-grained matrix composed of pinkish K-feldspar, whitish plagioclase, quartz and biotite. Rare plagioclase phenocrysts are rimmed by one or two biotite-rich rings. Quartz grains display even extinction and tend to form aggregates. Biotite is dark brown, with rare traces of chloritization. Scarce accessory minerals visible in thin-section are zircon and apatite.

4. Methods

4.1. Zircon separation

The studied c. 3 kg porphyritic granite sample was crushed, sieved, and the 0.06–0.25 mm heavy fraction separated using the conventional heavy liquid (sodium polytungstate) procedure. A hand-picked zircon separate was annealed and subjected to CA. Representative CA single grains were imaged at high magnification by SEM to investigate details of surface textures (Fig. 2). Hand-picked zircons representing slightly different morphological types from the untreated and from CA fractions were mounted in two separate epoxy pucks, polished and used for optical microscopy, cathodoluminescence (CL) imaging (Fig. 3) and, finally, SIMS analysis.

4.2. Chemical abrasion

The CA technique used in this study closely follows that described by Mattinson (2005) as a pre-treatment prior to TIMS analysis. An unpicked bulk zircon fraction was annealed at 850^{o}C in a covered quartz glass dish for 60 hours. Following this, the zircon crystals were ultrasonically washed in 4M HNO_3, rinsed in ultra-pure water, then further washed in warm 4M HNO_3 prior to rinsing with distilled water to remove any surface contamination. Annealed, cleaned bulk zircon fractions were then partially dissolved ("*chemically abraded*") in 200 µl 29M HF and 20 µl 8M HNO_3 in cleaned modified 0.5 ml Teflon© microcentrifuge tubes in a Parr™ bomb at 180^{o}C for 12 hours. After cooling, the HF- HNO_3 solution was pipetted off and the CA zircons were rinsed several times in ultra-pure water, cleaned in warm 3N HCl for several hours on a hotplate and rinsed again in ultra-pure water. Zircons treated in this manner were then pipetted in alcohol for preparation of a conventional epoxy puck.

The primary purpose of zircon thermal annealing is to seal up fission tracks, alpha-recoil tracks and micro-cracks (Mattinson, 2005), however larger-scale fractures are likely to remain open. High-U domains with considerable radiation damage are not fully annealed. Such metamict zircon is often largely or completely dissolved during the relatively low temperature CA. In this regard, the

process screens grains which have suffered severe radiation damage and Pb-loss. Mattinson (2005) demonstrated how annealed zircons behave during incrementally higher temperature partial dissolution steps. With each higher temperature step, a greater volume of the zircon will be dissolved, furthermore, the lower temperature leachates often contain the highest U concentrations. From this, it is intuitive that (i) when exposed to HF-HNO_3 vapour, the high-U (and other trace element-rich) zones will dissolve more readily, and (ii) higher temperatures will cause more aggressively partial dissolution. Whereas we have adopted a temperature of 180^{o}C for CA in this study, temperatures between 120 and 210^{o}C could be used, depending on the observed U concentrations and also the severity of partial dissolution anticipated to be required to effectively remove zones of Pb-loss.

4.3. SHRIMP analytical procedure

In-situ U–Pb analyses, both of the non-abraded and CA zircons, were performed on a SHRIMP-II at the Centre of Isotopic Research (CIR) at VSEGEI, St. Petersburg, Russia. A secondary electron multiplier in peak-jumping mode was applied, following the procedure described in Williams (1998) and Larionov et al. (2004). A primary beam of molecular oxygen was employed to ablate zircon in order to sputter secondary ions. The elliptical analytical spots had a size of c. 27 x 20 μm, and the corresponding primary ion current was c. 4 nA. The sputtered secondary ions were extracted at 10 kV. The 80 μm wide slit of the secondary ion source, in combination with a 100 μm multiplier slit, allowed mass-resolution of $M/\Delta M \geq 5000$ (1 % valley) so that all the possible isobaric interferences were resolved. One-minute rastering over a rectangular area of c. 120 μm was employed before each analysis in order to remove the gold coating and possible surface common Pb contamination.

The following ion species were measured in sequence: $^{196}(Zr_2O)$–^{204}Pb–background (c. 204.5 AMU) –^{206}Pb–^{207}Pb–^{208}Pb–^{238}U–^{248}ThO–^{254}UO with integration time ranging from 2 to 20 seconds. Four cycles for each analysis were acquired. Each fifth measurement was carried out on the TEMORA 1 zircon U/Pb standard (Black et al., 2003) The 91500 zircon (Wiedenbeck et al., 1995) was applied as a "U-concentration" standard. The collected results were then processed with SQUID v1.13a (Ludwig, 2005a) and ISOPLOT/Ex 3.22 (Ludwig, 2005b) software, using the decay constants of Steiger and Jäger (1977). The common lead correction was accomplished using measured ^{204}Pb according to the model of Stacey and Kramers (1975).

Uncertainties for individual analyses (ratios and ages) are given at the 1σ level, uncertainties in calculated mean ^{206}Pb/^{238}U ages are reported at 2σ level. The results of zircon analyses are shown in Tables 1 and 2 and in Figures 5 and 6.

4.4. Possible sources of SIMS inaccuracy

While poor counting statistics is considered to be the main factor of poor precision, inaccuracy may be attributed to other factors. A shift in ^{206}Pb/^{238}U ratio and, hence, apparent age, may result from:

1. common Pb correction to erroneous lead isotope composition, especially in ^{204}Pb-rich zircons;
2. Secondary Electron Multiplier (SEM) saturation (Williams and Hergt, 2000), such as that which is likely to occur when U concentrations exceed 5000 ppm producing an erroneous older age due to U/Pb undercounting. This effect may combine with perturbation of the U–Pb system through Pb-loss, occasionally giving a final value indistinguishable of "true age";
3. focus/extraction disturbance due to spontaneous sample movement (Black et al., 2004);
4. poor focus due to rigid surface;
5. remote position of unknown zircon relative to standard on a puck (Stern and Amelin, 2003);

6. difference in crater depth for unknowns and standards caused by different ablation rate or differences in analytical procedure;

7. compositional misfit to standard zircon, so-called "matrix effect" (Black et al., 2004). Such heterogeneities could be tiny inclusions or fractures contributing to such matrix effects.

8. zircon annealing at high temperatures (>900^{o}C) may induce formation of baddeleyite and redistribution of Pb within certain zones causing reverse discordance (McLaren et al., 1994).

9. Severe reverse discordance of untreated zircon analysed by SIMS has been documented by Wiedenbeck et al. (1995). This has been attributed to enhanced ion yields (relative to U yield) of labile radiogenic Pb present in amorphous microdomains within the zircon.

Any of these factors above may readily occur in U-rich, or metamict zircon. Indeed migration of trace elements, including lead, can easily occur in metamict zircon considering its destructed porous structure. While in pristine zircon, fractures and small inclusions (even unexposed) can easily be identified, e.g. in transmitted-light images, a metamict zircon may hide defects below its very surface being usually non-transparent.

Thus usually U-rich zircons are not generally the target of choice in SIMS geochronology. Summarizing the above, it may be concluded that if U-rich zircon dating is unavoidable, the data obtained should be controlled by other isotope techniques to provide extra evidence for age. In the case of the Karkonosze zircons, which are U- ^{204}Pb- and impurity- rich, all these factors may contribute to inaccuracy.

5. Detailed comparison of zircons before and after chemical abrasion

Zircons from sample SZH are morphologically very homogeneous and represented, almost entirely, by euhedral, normal- to long-prismatic crystals between c. 70-250 x 30-80 x 20-70 μm

(Fig. 3). In transmitted light, they are usually colourless, transparent to slightly turbid. Some of untreated euhedral crystals display obvious traces of former surface intergrowths or inclusions. Other surface features such as curvilinear fractures are also present. Irregular cracks and fissures are quite common and may be linked to the high U content of some of the zircons. No distinct cores are discernible optically but magmatic inclusions are also abundant.

In transmitted light, the CA zircons appear darker in colour and less transparent (Fig. 3). In reflected light and in BSE images, the polished surface of the CA crystals reveals many imperfections such as nets of irregular cracks and sets of grooves, the latter imitating the euhedral-shaped internal zoning. In SEM images (Fig. 2), the CA grains display some very different characteristics. The CA zircon population displays significant physical deterioration. Overall, the habit remains the same but crystals are mechanically weak and prone to disintegration during polishing. SEM images of CA grains reveal swarms of sub-micron pits and micro-channel networks of etched and dissolved pathways. In many cases, these appear to follow v-shaped patterns, or linear zones parallel to external surfaces. Crystallographic imperfections have been strongly accentuated by CA showing that indistinct cleavage and zoning boundaries appear to be weakened parts of the crystals being more easily damaged by metamictization and, consequently, prone to preferential dissolution. It is notable that although all grains have been subjected to the same thermal annealing and HF acid attack, some have been more aggressively attacked than others. Importantly, some dissolved pathways appear to penetrate through the entire zircon grain or follow 3D growth-zones. These images also illustrate how conventional HF acid vapour digestion of zircon is likely to proceed.

CL images reveal that the zircon population is also fairly homogeneous, with only rare distinct inherited cores (Fig. 3). Typically, the zircons are CL-dark, reflecting high U and Th contents. Many grains have CL-brighter internal parts, mostly parallel to the external euhedral habit, locally slightly rounded. These internal parts are irregularly structured, with CL-darker amoeboid patches.

CL imaging of CA grains demonstrate a number of features illustrating how CA has affected the zircons. Firstly, magmatic zoning is still present despite the high temperature of thermal annealing. This is due to the time required for diffusion of trace elements in zircon being far greater than the short duration of annealing (Cherniak and Watson, 2000). Importantly, the closure temperature for Pb in crystalline zircon (Lee et al., 1997) is such that the U–Pb isotopic system is not disturbed during this annealing process (Mattinson, 2005). CL images indicate that, in most cases, dark CL (high-U) zones have been selectively dissolved. As with the SEM images, this can be observed to have occurred in 3D, penetrating into the innermost portions of the crystals. Grains in the epoxy mount appear to be fragmented, this is largely an artefact of the plane at which they have been ground, polished and imaged, as undissolved zircon occurs at depth in the mount. Once being CA however, some grains appear as skeletal pseudomorphs of former entire grains and are extremely fragile (e.g. grains 30 and 33, Fig. 3). Crystals with partially dissolved linear zones cutting across the oscillatory zoning are also evident in the CL images. These are likely to represent micro-fractures along which fluids could have leached radiogenic lead from damaged zircon domains.

6. SHRIMP results

6.1. U–Pb SIMS data from untreated zircons

Twelve analyses in eleven zircon grains have been carried out (Table 1). Zircons display U and Th concentrations of generally 600–3 000 and 200–500 ppm respectively, with some high concentration anomalies (e.g. U c. 20 000 ppm and Th c. 1 600 ppm for spot 11.1). Measured Th/U is generally c. 0.2 and typical of magmatic zircons, but grain 11.1 with a low $^{232}Th/^{238}U$ ratio of 0.08, is likely of a very-late stage magmatic or possibly hydrothermal origin. Nine spots (1.1, 2.1,

3.1, 4.1, 5.1, 6.1, 7.1, 9.1, 2.2; Table 1) yield a mean $^{206}Pb/^{238}U$ age of 306±4 Ma (MSWD = 0.86, probability 0.55; Fig. 4). Three spots (8.1, 10.1, 11.1) gave $^{206}Pb/^{238}U$ ages younger than this main population, presumably due to Pb-loss. There is no apparent correlation between U and Th ppm and the degree of discordance. Common $^{206}Pb_c$ contents vary between 0.04 and 10.7 %.

6.2. U–Pb SIMS data from chemically abraded zircons

Sixteen analyses in thirteen abraded zircons were performed. The zircons are slightly variable in their geochemical characteristics with moderate to high U (175–1 377 ppm) and Th (81–506 ppm) concentrations (Table 2). $^{232}Th/^{238}U$ ratios generally vary between 0.2 and 0.5. The $^{206}Pb_c$ relative contributions are low, between 0 and 0.67 %. Comparing selected chemical features of the abraded zircons with those of the non-treated ones, it is obvious that the latter are, on average, much richer in U and Th, and often have elevated $^{206}Pb_c$. Overall, the $^{206}Pb/^{238}U$ ages of the abraded grains lie between c. 346 and c. 297 Ma (Fig. 5). The main cluster of 11 spots gives a mean $^{206}Pb/^{238}U$ age of 322±3 Ma (MSWD = 1.15, probability .0.32). Two spots (38.1 and 42.1; Table 2) have slightly older $^{206}Pb/^{238}U$ ages (c. 338); it is equivocal from CL images if these contain inherited cores. One spot (32.1), gives an older $^{206}Pb/^{238}U$ age of 346±6 Ma and the CL image for this grain indicates that it is likely to have an inherited core. Two spots (35.2 and 31) give apparent $^{206}Pb/^{238}U$ ages slightly younger than the main population cluster.

7. Possible causes of inaccuracy in U–Pb SIMS ages

7.1. Background on SIMS methodologies

It has long since been recognized that deviation from expected U–Pb ages, determined by ID-TIMS, can occur in microbeam dating techniques, including SIMS. Factors, other than Pb-loss, such as poor counting statistics, detector saturation, matrix standard - to - sample (mis-) matching (Black et al., 2004), threshold concentrations of trace elements (Williams and Hergt, 2000; Rasmussen and Fletcher, 2002), crystallographic direction orientation (Wingate and Compston, 2000) and crystal position on the mount (Stern and Amelin, 2003), have all been cited as possible causes of an observable bias in SIMS U–Pb dating. These are evaluated in turn as possible causes for the age discrepancy between sample SZH for untreated and CA zircons.

7.2. Matrix matching between standard and sample

In a study of matrix effects relating to U–Pb SIMS geochronology, Black et al. (2004) made a correlation of the extent of deviation from an expected (ID-TIMS) $^{206}Pb/^{238}U$ age with an elevation in the concentration of zircon trace elements. It was found that elevated levels of P, Sm and, in particular, Nd seem to have a direct correlation on the extent of the age bias. Using TEMORA 1 as a primary SHRIMP standard, Black et al. (2004) demonstrated that the $^{206}Pb/^{238}U$ age for certain zircon standards deviated in both a positive (SL13, R33, TEMORA 2) and negative (AS3) sense. There appears to be a reverse correlation, but not necessarily any direct cause, between sense of age offset with Nd concentration over a surprisingly narrow concentration range. For instance, Black et al. (2004) found that the zircon standard AS3, which has higher concentrations of Nd (c. 7 ppm) relative to TEMORA 1 (c. 3 ppm), displays a corresponding negative $^{206}Pb/^{238}U$ age offset of c. 1 % from the accepted TIMS age. Due to the fact that the limit on precision of $^{206}Pb/^{238}U$ SIMS data for zircon from the Karkonosze Granite in this study is in the order of 2 %, it is likely that only extreme differences in zircon Nd between the TEMORA 1 standard and analysed sample could be linked with any recognisable apparent age offset effect.

For this study, the zircon U–Pb standard TEMORA 1 with an accepted $^{206}Pb/^{238}U$ age of 416.75 ±0.24 Ma (Black et al., 2003) was used as Pb-U standard for both analytical sessions. Selected REE (Nd, Sm, Eu, Gd, Yb, Lu) and Hf analysis of ten representative zircons was carried out at the University of Bristol using laser ablation ICP-MS (analytical details to be published by the University of Bristol Laboratory team). These were analysed from the same grain mounts used for U–Pb SIMS geochronology. In general, untreated zircons have an order of magnitude higher concentration of Nd when compared to the CA set (Table 3). No micro-inclusions of U-rich REE bearing minerals (e.g. xenotime, monazite) are visible in SEM images of the analysed zircons, but it is possible that these would occur at a scale not resolvable using this imaging technique. It is unclear whether partial dissolution has resulted in large-scale leaching of REE, or effective removal of the higher U domains has had a similar effect on REE-rich zones, or micro-inclusions. Although it is evident that the non-treated zircons display younger apparent ages, it is perhaps more likely that this has resulted from Pb-loss, rather than some effect associated with higher Nd concentration. The rationale supporting this, comes from a lack of systematic correlation between apparent $^{206}Pb/^{238}U$ ages and Nd concentration, despite the large variations in Nd concentration in both the CA (8–52 ppm Nd) and non-treated (122–658 ppm Nd, with one outlier of 18 ppm Nd) zircons (Table 3).

7.3. Threshold concentrations of trace elements

The 91500 zircon with a U concentration of 81.2 ppm and a $^{206}Pb/^{238}U$ age of 1062.4±0.4 Ma (Wiedenbeck et al., 1995) was applied as a U-concentration standard for this study. The U concentration of zircons from sample SZH is considerably higher than that of the standard. The high U concentration of zircons, such as that observed in zircons from the Karkonosze Granite, is a problematic factor in SIMS dating. There is a lack of suitable and readily available natural standard material in this concentration range. Williams and Hergt (2000) have stated that for SIMS dating, a

threshold value above 2 500 ppm U creates a measureable shift in $^{206}Pb/^{238}U$ age due to detector saturation. This has been quantified as approximately a 1.5 to 2.0 % increase in $^{206}Pb/^{238}U$ age for every additional 1 000 ppm of U. Whereas no zircons from the CA bulk fraction have U concentrations in excess of this, grains 6.1 and 11.1 from the untreated aliquot attain c. 3 500 and 20 000 ppm, respectively. Results from several other grains from the untreated sample approach the 2 500 ppm U threshold (spots 1.1, 2.1, 5.1, 7.1). Perhaps it is significant that grain 6.1 from the untreated sample yields the oldest apparent $^{206}Pb/^{238}U$ age (315.9 ±5.1 Ma), whereas the remainder of the statistically coherent untreated population have apparent $^{206}Pb/^{238}U$ ages between c. 300 and 310 Ma. Although it is recognised that high U concentrations may cause a positive bias in ages determined, the higher U concentrations in the larger expected radiation damage and Pb-loss, which yields younger apparent ages. It is likely that there is a complex and unquantifiable interplay between a positive apparent age bias and Pb-loss in some of the high-U zircon grains. The CL images of CA grains show the process may be used as a screening tool whereby high-U zones are preferentially partially dissolved. Taking this process to an extreme, high-U grains may be entirely dissolved where this would be an advantageous outcome to screen for or eliminate zircons unsuitable for U–Pb SIMS geochronology.

7.4. Age bias in relation to puck edge effect

In a comprehensive study of SIMS analysis error sources, Stern and Amelin (2003) documented a previously unknown phenomenon relating to a shift in measured U–Pb ratios in proximity to puck edge. Fragments of a natural zircon standard (Sri Lankan zircon megacryst Z6266), considered to be homogenous as proved by TIMS analysis of separate aliquots, were mounted in a grid-like fashion and $^{206}Pb/^{270}UO_2$ was analysed by SHRIMP applying atomic O^- primary beam. A systematic discrepancy in the measured ratio in relation to the position of standard chips on the mount has been

found. This effect was seen to be most extreme at the edges of the 10 mm diameter area where measured ratios could deviate by as much as c. 1.6 % from edge to edge in the Y-steering (horizontal) direction.

Our study compares U–Pb data from two grain mounts whereby the analysed grains were positioned in the central portion of each mount and unknowns have been mounted just next to standards. In this regard there should not be any discernable bias in the measured ratios due to "edge-effects". Moreover, the observed age discrepancy between the separate mounts (c. 6 %) is far greater than could reasonably be attributed to even the most extreme spatially correlated variations.

8. Discussion

There have been several attempts to obtain meaningful emplacement ages for the Karkonosze Granite. Previous U–Pb zircon dating attempts, using a range of techniques, have yielded apparent ages between c. 302-319 Ma, while a cross cutting dyke limits a minimum age to c. 313 - 318 Ma (Awdankiewicz et al., 2010). A main factor contributing to the difficulties faced seems to be the chemical features of the zircons, namely the elevated U and Th contents (600–1 300 ppm U in the untreated population). With such high concentrations of radioactive elements, the zircons are prone to structural damage, metamictization and consequently disturbance of the U–Pb isotopic system. Utsunomiya et al. (2007) have shown that heavily metamictized high U and Th zones in zircons also have higher concentrations of trace element impurities (e.g. Ca, Al) and secondary alteration nano-phases. Although some "ambient annealing" of zircon could occur over geological timescales and under suitable conditions (Nasdala et al., 2001), once a point of interconnectivity of amorphous radiation damaged zones has been attained, Pb-loss can occur. Indeed, metamictization accelerates diffusion of Pb in radiation damaged zones (Cherniak et al., 1991) and allows leaching by various

fluids (Davis and Krogh, 2000; Breeding et al., 2004). A pronounced influence of late-magmatic fluids on re-equilibration of zircons from a microgranular enclave in the Karkonosze Granite has recently been shown by Kusiak et al. (2009). The zircons that originally crystallised during mingling of mafic magma into a cooler granitic melt display unusual morphologies and re-equilibration textures, such as corrosion and replacement by microgranular aggregates of zircon and thorite, attributed to the action of late-magmatic fluids. The fluid activity, dated at c. 304±3 Ma, is interpreted to postdate the magmatic emplacement of the main part of the pluton by several million years (Kusiak et al., 2009). However, thermochronology of the Karkonosze Granite zircons (Danišík et al., 2010) suggests that temperatures below 190^{o}C were reached between 295 ± 20 and 308 ± 21 Ma. This would mean either relatively cold fluids or underestimation of age by Kusiak et al. (2009).

In our experiment, the artificial thermal annealing of representative grains followed by partial dissolution has resulted in visible physical changes. Most importantly, the U- and Th-rich domains seem to have been preferentially attacked and in some cases removed, leaving only the least disturbed or undisturbed parts of crystals. There is a clear difference in U–Pb SHRIMP datasets for untreated and CA zircon grains. A statistically coherent population of CA grains gives a weighted mean $^{206}Pb/^{238}U$ age of 322±3 Ma, which is c. 5 % older than that obtained from the untreated grains but fits well with age data from other isotope studies. There are a number of possible causes for $^{206}Pb/^{238}U$ age bias in SIMS geochronology, however it would appear that here such an age bias can be predominantly ascribed to the effects of remobilisation and Pb-loss. Significantly, it is not possible to statistically recognise Pb-loss in the main population of untreated zircons. If these analyses were to be taken in isolation (and ignoring other constraints, e.g. Ar–Ar and Rb–Sr data, and the c. 313-318 Ma U–Pb zircon age of a cross-cutting dyke), it could be assumed that 306±3 Ma represents a true magmatic crystallisation age for the Karkonosze Granite. However, comparison with U–Pb dating of the CA grains indicates that the entire untreated population has

suffered a notable amount of Pb-loss. It may be the case that this would have been recognised with higher precision analyses (e.g. < 0.1 % 2σ error achievable with ID-TIMS), but in terms of a routine level of precision attained by SIMS (c. 1–2 % per analysis), this example clearly identifies a real possibility that such cryptic Pb-loss would not be readily evident. Chemical abrasion of zircons has also resulted in visible removal of inclusions and presumably also the alteration products resulting in lower common lead.

Given that some analyses from the CA zircons lie on a Pb-loss trajectory from c. 324 Ma, we can deduce that the procedure as described has not fully removed metamict Pb-lost domains from every analysed grain, however it has reduced the overall volume of affected zircon within the treated population. An investigation into radiation damage in natural zircon (Nasdala et al., 2005) has shown that sites of high alpha particle impact/recoil damage can occur in low actinide zones where they have originated from adjacent zones with higher U and Th. Bearing in mind that the partial dissolution procedure preferentially attacks high-U zones in the zircons, it is possible that some residual effects of Pb-loss due to alpha radiation in the relatively lower U zones may remain. It is feasible that partial dissolution at higher temperatures would have been more effective in removing damaged portions of zircons hence resulting in a more effective removal of the Pb-loss effects from all the grains. Given the relatively high concentration of U in the sample however, higher temperatures were not utilized as this may have resulted in complete dissolution of the zircons. This is supported by the observation that treated grains generally have lower U concentration, suggesting that higher U zircon have already been dissolved. Given that a bulk fraction was treated however, the extent of total dissolution of grains cannot be quantified.

9. Conclusion

Although the CA technique was originally developed as a utility to eliminate or minimise the effects of Pb-loss in zircon for ID-TIMS, we demonstrated it's applicability to SIMS U–Pb geochronology. The CA technique, which is now widely accepted as the most robust pre-treatment tool for high-precision TIMS U–Pb chronology (Mundil et al., 2004; Mattinson, 2005; Mattison et al., 2006), has not previously been demonstrated to be effective in micro-beam techniques. Using a population of zircons from the Karkonosze Granite (SW Poland), we illustrate that a modified CA procedure is beneficial in:

1) Cleansing or removing domains which were prone to lead loss, mainly due to chemical impurities, and imperfections in the zircon lattice (radiation damage). This treatment allows retention less- or undisturbed zircon domains for analysis, thus significantly reducing the effects of Pb-loss on the U–Pb chronometer.
2) Dramatically reducing the amounts of non-radiogenic ("common") lead, via preferential dissolution of domains containing high common Pb (e.g. magmatic inclusions) and micro-mineral inclusions which may also contain relatively high amounts of initial common lead, Y and REE. CA also removes any "unsupported" lead which might have entered the grains along cracks or contaminated "spongy" domains within grains.

Consequently, the CA method allows us to make analytical results more accurate. The overall effect is a significant improvement in age accuracy, as has been demonstrated in CA-TIMS.

Importantly, the CA approach has an additional benefit when applied to in situ methods, because it may reduce, to a negligible level, the effects of partial lead loss analysed micro-domains. This effect is readily recognisable in severe cases but, as our untreated zircon population demonstrates, can by cryptic and impossible to identify without reference to another technique or robust isotope system. In so doing, this technique can potentially greatly improve the accuracy of the measured ages, which otherwise may lag far behind the quoted precisions.

Reducing the influence of open (i.e. discordant) domains through selective dissolution is a valuable pre-treatment to any analytical method used to calculate U–Pb ages. It may prove to be of even more crucial importance when micro-beam techniques are used to date Phanerozoic zircons. This is because, unlike ID-TIMS, which is capable of producing 0.1 % error ellipses allowing recognition of slightly discordant data, the spatially resolved methods do not consume in this case enough sample volume to measure ^{207}Pb with a precision sufficient to assess correctly the degree of discordance of the U–Pb system in the analysed spot. As discussed by Pin and Rodriguez (2009), this may lead to consider as concordant (that is, documenting a closed system), and by inference geologically significant, $^{206}Pb/^{238}U$ and $^{207}Pb/^{235}U$ ages which are in fact slightly, but significantly, discordant due to radiogenic lead loss, thereby biasing the quoted date towards too young values. This potential pitfall of "spurious concordance", purely caused by the poor analytical precision of $^{207}Pb/^{235}U$ ratios, is an intrinsic limitation of *in situ* U-Pb methods when applied to relatively young samples. Removing discordant domains prior to *in situ* analysis by using "chemical abrasion" offers an effective means to minimize this source of inaccuracy.

Acknowledgements

This research was carried out under the Project MNiI 5T12B 036 25 of the Polish National Research Committee (KBN). Additional support came from internal grants 1017/S/ING and 2022/W/ING of the University of Wrocław. Thanks to Anna Pietranik and the University of Bristol Lab team for performing laser ablation ICP-MS analyses of Hf and REE in zircons, and to Grenville Turner (BGS) for providing SEM zircon images.

References

Ashwal, L., Armstrong, R., Roberts, R., Schmitz, M., Corfu, F., Hetherington, C., Burke, K., Gerber, M., 2007. Geochronology of zircon megacrysts from nepheline-bearing gneisses as constraints on tectonic setting: implications for resetting of the U–Pb and Lu–Hf isotopic systems. Contributions to Mineralogy and Petrology 153/4, 389–403.

Awdankiewicz, M., 2007. Late Palaeozoic lamprophyres and associated mafic subvolcanic rocks of the Sudetes (SW Poland): petrology, geochemistry and petrogenesis. Geologia Sudetica 39, 11–97.

Awdankiewicz, M., Awdankiewicz, H., Kryza, R., Rodionov, N., 2010. SHRIMP zircon study of a micromonzodiorite dyke in the Karkonosze Granite, Sudetes (SW Poland): age constraints for late Variscan magmatism in Central Europe. Geological Magazine 147, 77–85.

Barbarin, B., 1999. A review of the relationships between granitoids types, their origins and their geodynamic environments. Lithos 46, 605–626.

Black L.P., Kamo, S.L., Allen, C.M., Aleinikoff, J.N., Davis, D.W., Korsch, R.J., Foudoulis, C., 2003. TEMORA 1: a new zircon standard for Phanerozoic U–Pb geochronology. Chemical Geology 200, 155–170.

Black, L.P., Kamo, S.L., Allen, C.M., Davis D.W., Aleinikoff, J.N., Valley, J.W., Mundil, R., Campbell, I.H., Korsch, R.J., Williams, I.S., Foudoulis, C., 2004. Improved $^{206}Pb/^{238}U$ microprobe geochronology by the monitoring of a trace-element-related matrix effect; SHRIMP, ID–TIMS, ELA–ICP–MS and oxygen isotope documentation for a series of zircon standards. Chemical Geology 205, 115–140.

Borkowska, M., 1966. Petrografia granitu Karkonoszy. Geologia Sudetica 2, 7–119. (in Polish, French summary).

Breeding, C.M., Ague, J.J., Grove, M., Rupke, A.L., 2004. Isotopic and chemical alteration of zircon by metamorphic fluids: U–Pb age depth-profiling of zircon crystals from Barrow's garnet zone, northeast Scotland. American Mineralogist 89, 1067–1077.

Chaloupský, J., Červenka, J., Jetel, J., Králik, F., Libalová, J., Přchová, E., Pokorný, J., Pošmourný, K, Sekyra, J., Shřbený, O., Šalanský, K., Šrámek, J. & Václ, J., 1989. Geology of the Krkonoše and Jizerské hory Mts. Ústředni ústav geologický, Praha, 1–288. (in Czech, English summary).

Cherniak, D.J., Lanford, W.A., Ryerson, F.J., 1991. Lead diffusion in apatite and zircon using ion implantation and Rutherford backscattering techniques. Geochimica et Cosmochimica Acta 55, 1663–1673.

Cherniak, D.J., Watson, E.B., 2000. Pb diffusion in zircon. Chemical Geology 172, 5– 24.

Closs, H., 1925. Einführung in die tektonische Behandlung magmatischer Erscheinungen (Granittektonik). I Spez. Teil. Das Riesengebirge in Schlesien, Berlin, 1–194.

Danišík, M., Migoń, P., Kuhlemann, J., Evans, N.J., Dunklf, I., Frisch, W., 2010. Thermochronological constraints on the long-term erosional history of the Karkonosze Mts., Central Europe. Geomorphology 117 (1-2), 78– 89.

Davis, D.W., Krogh, T.E., 2000. Preferential dissolution of 234U and radiogenic Pb from α-recoil-damaged lattice sites in zircon: implications for thermal histories and Pb isotopic fractionation in the near surface environment. Chemical Geology 172, 41–58.

Diot, H., Mazur, S., Couturie, J. P., 1994. Magmatic structures in the Karkonosze granite and their relation to tectonic structures in the eastern metamorphic cover. In: Kryza R. (Ed.), Igneous activity and metamorphic evolution of the Sudetes area. Conference Abstracts, Wrocław University, 36–39.

Duthou, J.L., Couturie, J.P., Mierzejewski, M.P., Pin, C., 1991. Next dating of granite sample from the Karkonosze Mountains using Rb–Sr total rock isochrone method. Przegląd Geologiczny 36, 75–79. (in Polish, English summary).

Klominsky, J., 1969. The Krkonoše–Jizera granitoid massif. Sborník geologických věd 15, Praha, 1–134.

Krogh, T.E., 1982. Improved accuracy of U–Pb zircon ages by the creation of more concordant systems using an air abrasion technique. Geochimica et Cosmochimica Acta 46, 637–649.

Krogh, T.E., Davis, G.L., 1974. Alteration in zircons with discordant U–Pb ages. Carnegie Institution Yearbook 73, 560–567.

Krogh, T.E., Davis, G.L., 1975. Alteration in zircons and differential dissolution of altered and metamict zircon. Carnegie Institution Yearbook 74, 619–623.

Kröner, A., Hegner, E., Hammer, J., Haase, G., Bielicki, K-H., Krauss, M., Eidam, J., 1994. Geochronology and Nd–Sm systematics of Lusatian granitoids: significance for the evolution of the Variscan orogen in east-central Europe. Geologische Rundschau 83, 357–376.

Kryza, R., Mazur, S., Oberc-Dziedzic, T., 2004. The Sudetic geological mosaic: insights into the root of the Variscan orogen. Przegląd Geologiczny 52, 761–773.

Kusiak, M.A., Dunkley, D.J., Słaby, E., Budzyń, B., Martin, H., 2008. U–Pb chronology of zircon from granites of the Karkonosze Pluton, NE Bohemian Massif. 4th SHRIMP workshop. Saint Petersburg, Russia, Abstract Volume, 70–80.

Kusiak, M.A., Dunkley, D.J., Słaby, E., Martin, H., Budzyń, B., 2009. Sensitive high-resolution ion microprobe analysis of zircon reequilibrated by late magmatic fluids in a hybridized pluton. Geology 37/12, 1063–1066.

Larionov, A.N., Andreichev, V.A., Gee, D.G., 2004. The Vendian alkaline igneous suite of northern Timan: ion microprobe U–Pb zircon ages of gabbros and syenite. In: Gee, D.G., Pease, V.L. (Eds.). The Neoproterozoic Timanide Orogen of Eastern Baltica. Geological Society London Memoirs 30, 69–74.

Lee, J.K.W., Williams, I.S., Ellis, D.J., 1997. Pb, U, and Th diffusion in natural zircon. Nature 390, 159–162.

Ludwig, K.R., 2005a. SQUID 1.12 A User's Manual. A Geochronological Toolkit for Microsoft Excel. Berkeley Geochronology Center Special Publication, 1–22. http://www.bgc.org/klprogrammenu.html

Ludwig, K.R., 2005b. User's Manual for ISOPLOT/Ex 3.22. A Geochronological Toolkit for Microsoft Excel. Berkeley Geochronology Center Special Publication, 1–71. http://www.bgc.org/klprogrammenu.html

Machowiak, K., Armstrong, R., 2007. SHRIMP U–Pb zircon age from the Karkonosze granite. Mineralogia Polonica. Special Papers 31, 193–196.

Marheine, D., Kachlik, V., Maluski, H., Patocka, F., Żelaźniewicz, A., 2002. New $^{40}Ar/^{39}Ar$ ages in the West Sudetes (Bohemian Massif): constraints on the Variscan polyphase tectonothermal development. In: Winchester, J.A., Paharaoh, T.C., Verniers, J. (Eds.), Palaeozoic Amalgamation of Central Europe. Geological Society Special Publication 201, 133–155.

Mattinson, J.M., 1994. A study of complex discordance in zircons using step-wise dissolution techniques. Contributions to Mineralogy and Petrology 116, 117–129.

Mattinson, J.M., 2005. Zircon U–Pb chemical abrasion ("CA-TIMS") method: Combined annealing and multi-step partial dissolution analysis for improved precision and accuracy of zircon ages. Chemical Geology 220, 47–66.

Mattinson, J.M., Hourigan, J., Wooden, J.L., 2006. Better U-Pb zircon standards for SIMS and LA-ICPMS? Preliminary results of detailed characterization and pre-treatment using CA-TIMS. Eos Trans. AGU, 87(52), Fall Meet. Suppl., Abstract V21A-0559.

McClelland, W.C., Mattinson, J.M., 1996. Resolving high precision U–Pb ages from Tertiary plutons with complex zircon systematics. Geochimica et Cosmochimica Acta 60 (20), 3955–3965.

McLaren, A.C., Fitz Gerald, J.D., Williams, I.S., 1994. The microstructure of zircon and its influence on the age determination from Pb/U isotopic ratios measured by ion microprobe. Geochimica et Cosmochimica Acta 58, 2, 993–1005.

Mazur, S., 1995. Structural and metamorphic evolution of the country rocks at the eastern contact of the Karkonosze granite in the southern Rudawy Janowickie Mts and Lasocki Range (in Polish with English summary). Geologia Sudetica 29, 31–98.

Mazur, S., Aleksandrowski, P., 2001. The Tepla(?)/Saxothuringian suture in the Karkonosze-Izera Massif, Western Sudetes, Central European Variscides. International Journal of Earth Sciences 90, 341–360.

Mazur, S., Aleksandrowski, P., Kryza, R., Oberc-Dziedzic, T., 2006. The Variscan Orogen in Poland. Geological Quarterly 50, 89–118.

Mierzejewski, M., Oberc-Dziedzic, T., 1990. The Izera-Karkonosze Block and its tectonic development (Sudetes, Poland). Neues Jahrbuch für Geologie und Paläontologie Abhandlungen 179, 197–222.

Mundil, R., Ludwig, K.R., Metcalfe, I., Renne, P.R., 2004. Age and timing of the Permian mass extinctions: U/Pb dating of closed-system zircons. Science 305, 1760–1763.

Nasdala, L., Wenzel, M., Vavra, G., Irmer, G., Wenzel, T., Kober, B., 2001. Metamictisation of natural zircon: accumulation versus thermal annealing of radioactivity-induced damage. Contributions to Mineralogy and Petrology 141, 125–144.

Nasdala, L., Hanchar, J.M., Kronz, A., Whitehouse, M.J., 2005. Long-term stability of alpha particle damage in natural zircon. Chemical Geology 220, 83–103.

Oberc-Dziedzic, T., 2003. The Izera granites: an attempt of the reconstruction of predeformational history. In: Ciężkowski, W., Wojewoda, J., Żelaźniewicz, A. (Eds.), Sudety Zachodnie: od wendu do czwartorzędu. WIND, Wrocław, 41–52. (in Polish, English summary).

Oberc-Dziedzic T., Kryza R., Mochnacka K., Larionov A., 2010: Ordovician passive continental margin magmatism in the Central-European Variscides: a case study from the SE part of the Karkonosze-Izera Massif, Polish Sudetes". International Journal of Earth Sciences 99, 27–46.

Pidgeon, R.T., Nemchin, A.A. 2006. High abundance of early Archaean grains and the age distribution of detrital zircons in a sillimanite-bearing quartzite from Mt Narryer, Western Australia. Precambrian Research 150, 201–220.

Pin, C., Mierzejewski, M.P., Duthou, J.L., 1987. Isochronous age Rb/Sr of Karkonosze granite from the quarry Szklarska Poręba Huta and significance of initial $^{87}Sr/^{86}Sr$ in this granite (in Polish with English summary). Przegląd Geologiczny 10, 512–517.

Pin, C., Rodriguez, J., 2009. Comment on "Rheic Ocean ophiolitic remnants in southern Iberia questioned by SHRIMP U-Pb zircon ages on the Beja-Acebuches amphibolites" by A. Azor A. et al., Tectonics 28, TC5013, doi:10.1029/2009TC002495.

Rasmussen, B., Fletcher, I.R., 2002. Indirect dating of mafic intrusions by SHRIMP U–Pb analysis of monazite in contact metamorphosed shale: an example from the Palaeoproterozoic Capricorn Orogen, Western Australia. Earth and Planetary Science Letters 197, 287–299.

Słaby, E., Martin, H., 2008. Mafic and Felsic Magma Interaction in Granites: the Hercynian Karkonosze Pluton (Sudetes, Bohemian Massif). Journal of Petrology 49, 353–391.

Słaby, E., Galbarczyk-Gąsiorowska, L., Seltmann, R., Müller, A., 2007. Alkali feldspar megacryst growth: Geochemical modeling. Mineralogy and Petrology 89, 1–29.

Stacey, J.S., Kramers, J.D., 1975. Approximation of terrestrial lead isotope evolution by a two-stage model. Earth and Planetary Science Letters 26, 207–221.

Steiger, R.H., Jäger, E., 1977. Subcommission on geochronology: convention on the use of decay constants in geo- and cosmochronology. Earth and Planetary Science Letters 36, 359–362.

Stern, R.A., Amelin, Y., 2003. Assessment of errors in SIMS zircon U–Pb geochronology using a natural zircon standard and NIST SRM 610 glass. Chemical Geology 197, 111–146.

Tilton, G.R., Patterson, C.C., Brown, H., Inghram, M., Hayden, R., Hess, D., Larsen Jr., E., 1955. Isotopic composition and distribution of lead, uranium, and thorium in a Precambrian granite. Geological Society of America Bulletin 66, 1131–1148.

Todt, W., Büsch, W., 1981. U–Pb investigations on zircons from pre-Variscan gneisses - I. A study from the Schwarzwald, West Germany. Geochimica et Cosmochimica Acta 45, 1789–1801.

Utsunomiya, S., Valley, J.W. Cavosie, A.J., Wilde S.A., Ewing R.C., 2007. Radiation damage and alteration of zircon from a 3.3 Ga porphyritic granite from the Jack Hills, Western Australia. Chemical Geology 236, 92–111.

Wetherill, G.W., 1956. Discordant uranium–lead ages. Trans. American Geophysical Union 37, 320–326.

Wiedenbeck, M., 1995. An example of reverse discordance during ion microprobe zircon dating: An artifact of enhanced ion yields from a radiogenic labile Pb. Chemical Geology 125, 197–218.

Wiedenbeck, M., Allé, P., Corfu, F., Griffin, W.L., Meier, M., Oberli, F., Von Quadt, A., Roddick, J.C., Spiegel, W., 1995. Three natural zircon standards for U–Th–Pb, Lu–Hf, trace element and REE analyses. Geostandards Newsletter 19, 1–23.

Wilamowski, A., 1998. Geotectonic environment of the Karkonosze and Tatra granite intrusions based on geochemical data. Archiwum Mineralogiczne 51, 261–271. (in Polish, English abstract).

Williams, I.S., 1998. U–Th–Pb Geochronology by ion microprobe. In: Applications in microanalytical techniques to understanding mineralizing processes. Reviews in Economic Geology 7, 1–35.

Williams, I.S., Hergt, J.M., 2000. U–Pb dating of Tasmanian dolerites: a cautionary tale of SHRIMP analysis of high-U zircon. In: Woodhead, J.D., Hergt, J.M., Noble, W.P. (Eds.),

Beyond 2000: New Frontiers in Isotope Geoscience, Lorne, 2000, Abstracts and Proceedings, pp. 185–188, University of Melbourne, Australia.

Wingate, M.T.D., Compston, W., 2000. Crystal orientation effects during ion microprobe U–Pb analysis of baddeleyite. Chemical Geology 168, 75–97.

Ţák, J., Klomínský, J., 2007. Magmatic structures in the Krkonoše–Jizera Plutonic Complex, Bohemian Massif: evidence for localized multiphase flow and small-scale thermal–mechanical instabilities in a granitic magma chamber. Journal of Volcanology and Geothermal Research 164, 254–267.

Figure Captions

Fig. 1. Geological sketch map of the Karkonosze-Izera Massif (compiled basing on Chaloupský, 1989; Mazur, 1995; Mazur and Aleksandrowski, 2001; Oberc-Dziedzic, 2003; Oberc-Dziedzic et al., 2010). KIM – Karkonosze-Izera Massif. Inset map: EFZ – Elbe Fault Zone, ISF – Intra-Sudetic Fault, MGH – Mid-German High, MO – Moldanubian Zone, MS – Moravo-Silesian Zone, NP – Northern Phyllite Zone, OFZ – Odra Fault Zone, RH – Rhenohercynian Zone, SBF – Sudetic Boundary Fault, SX – Saxothuringian Zone, TB – Teplá-Barrandian Zone. Rectangle shows the position of the KIM in the Bohemian Massif.

Fig. 2. SEM images of selected zircon crystals from sample SZH after chemical abrasion.

Fig. 3. Optical (transmitted light), BSE and CL images of selected non-abraded and chemically-abraded zircons, sample SZH; analytical spots (ellipses) are shown and $^{206}Pb/^{238}U$ ages given in labels.

Fig. 4. Concordia diagram for the non-abraded sample. Spot analyses shown as grey ellipses are not used in calculation of the reported mean $^{206}Pb/^{238}U$ age.

Fig. 5. Concordia diagram for the chemically-abraded sample. Spot analyses shown as grey ellipses are not used in calculation of the reported mean $^{206}Pb/^{238}U$ age.

Table Captions

Table 1

SHRIMP data for non-abraded sample SZH.

Table 2

SHRIMP data for chemically-abraded sample SZH.

Table 3

Laser ablation analyses of Hf and selected REE for abraded sample SZH (in ppm).

Table 1
SHRIMP data for non-abraded sample SZH.

Spot Name	% $^{206}Pb_c$	ppm U	ppm Th	$^{232}Th/^{238}U$	ppm $^{206}Pb^*$	(1)Age $^{206}Pb/^{238}U$ M.y.	±	(1)Age $^{207}Pb/^{206}Pb$ M.y.	±	%D	(1) $^{207}Pb^*/^{206}Pb^*$	±, %	(1) $^{207}Pb^*/^{235}U$	±, %	(1) $^{206}Pb^*/^{238}U$	±, %	err corr
10.1	0.46	644	213	0.34	19.7	224.5	3.9	209.0	101	-7	.0503	4.4	0.246	4.7	.0354	1.8	.377
11.1	0.19	20322	1616	0.08	658	237.9	3.9	330.1	19	39	.0530	0.8	0.275	1.9	.0376	1.7	.895
8.1	0.59	3031	492	0.17	119	286.8	4.6	351.6	48	23	.0535	2.1	0.336	2.7	.0455	1.6	.615
2.1	10.7	2322	436	0.19	106.4	300.0	5.1	334.6	202	12	.0531	8.9	0.349	9.1	.0476	1.7	.192
5.1	2.32	2233	420	0.19	93.8	300.8	5.0	356.4	204	18	.0537	9.0	0.353	9.2	.0478	1.7	.186
4.1	2.18	1620	410	0.26	68.7	304.0	5.0	342.0	101	13	.0533	4.5	0.355	4.8	.0483	1.7	.354
1.1	0.37	2483	316	0.13	104	304.7	4.9	361.9	50	19	.0538	2.2	0.359	2.8	.0484	1.7	.596
3.1	0.04	1613	223	0.14	67.1	305.0	4.9	313.2	31	3	.0526	1.4	0.352	2.2	.0484	1.7	.769
7.1	0.83	2038	362	0.18	85.6	305.2	4.9	304.8	61	0	.0524	2.7	0.351	3.1	.0485	1.7	.529
2.2	3.85	693	168	0.25	30.1	306.6	5.6	311.5	240	2	.0526	10.5	0.353	10.7	.0487	1.9	.175
9.1	8.83	639	130	0.21	29.7	310.4	6.8	350.8	481	13	.0535	21.3	0.364	21.4	.0493	2.2	.105
6.1	0.77	3474	1178	0.35	151	315.9	5.1	315.2	47	0	.0527	2.1	0.365	2.7	.0502	1.6	.619
Av. Pb_c	2.6 %																

Errors are 1-sigma; Pb_c and Pb^* indicate the common and radiogenic portions, respectively.

Error in Standard calibration was 0.48% (not included in above errors but required when comparing data from different mounts).

(1) Common Pb corrected using measured ^{204}Pb.

Table 2
SHRIMP data for abraded sample SZH.

Spot Name	% $^{206}Pb_c$	ppm U	ppm Th	$^{232}Th/^{238}U$	ppm $^{206}Pb^*$	(1)Age $^{206}Pb/^{238}U$ M.y.	±	(1)Age $^{207}Pb/^{206}Pb$ M.y.	±	%D	(1) $^{207}Pb^*/^{206}Pb^*$	±, %	(1) $^{207}Pb^*/^{235}U$	±, %	(1) $^{206}Pb^*/^{238}U$	±, %	err corr
35.2	0.24	175	159	0.94	7.09	297.0	7.3	294.0	120	-1	.0522	5.2	0.339	5.8	.0471	2.5	.434
30.1	0.17	878	506	0.60	36.2	301.4	5.6	281.0	68	-7	.0519	3	0.343	3.5	.0479	1.9	.538
35.1	0.17	895	168	0.19	38.5	314.3	5.2	293.0	34	-7	.0522	1.5	0.359	2.3	.0500	1.7	.749
39.1	0.30	581	127	0.23	25.1	315.9	5.0	255.0	71	-19	.0513	3.1	0.355	3.5	.0502	1.6	.468
30.2	0.00	1216	265	0.22	52.7	317.5	4.9	205.0	33	-35	.0502	1.4	0.350	2.1	.0505	1.6	.749
40.1	0.17	470	204	0.45	20.5	319.1	5.2	319.0	62	0	.0528	2.7	0.369	3.2	.0508	1.7	.521
31.1	0.67	193	81	0.43	8.52	320.3	5.6	483.0	150	51	.0568	6.7	0.399	6.9	.0509	1.8	.261
34.1	0.30	585	103	0.18	25.8	321.5	5.6	239.0	75	-26	.0510	3.2	0.359	3.7	.0511	1.8	.486
33.1	0.61	443	171	0.40	19.8	324.5	5.3	306.0	110	-6	.0525	4.6	0.374	4.9	.0516	1.7	.340
41.1	0.14	1190	240	0.21	53.1	326.2	5.4	323.0	37	-1	.0529	1.6	0.378	2.4	.0519	1.7	.722
37.1	0.67	373	107	0.30	16.8	327.0	6.3	359.0	130	10	.0537	5.7	0.385	6.1	.0520	2	.327
36.1	0.32	253	99	0.41	11.4	328.8	5.5	413.0	87	26	.0550	3.9	0.397	4.2	.0523	1.7	.403
32.2	0.33	1377	372	0.28	62.7	331.8	5.2	332.0	50	0	.0531	2.2	0.387	2.7	.0528	1.6	.584
38.1	0.51	774	171	0.23	35.9	337.1	5.4	396.0	76	17	.0546	3.4	0.404	3.7	.0537	1.6	.438
42.1	0.20	1211	291	0.25	56.1	337.8	5.3	383.0	50	13	.0543	2.2	0.403	2.8	.0538	1.6	.584
32.1	0.02	727	197	0.28	34.4	345.9	5.5	370.0	39	7	.0540	1.7	0.410	2.4	.0551	1.6	.689
Av. Pb_c	0.30%																

Errors are 1-sigma; Pb_c and Pb^* indicate the common and radiogenic portions, respectively.

Error in TEMORA Standard calibration was 0.54% (Average of 14).

(1) Common Pb corrected using measured ^{204}Pb.

Table 3
Laser ablation analyses of Hf and selected REE for abraded sample SZH (in ppm).

	Non-abraded					**Abraded**				
	SZH 1.1	SZH 9.1	SZH 3.1	SZH 10.1	SZH 6.1	SZH 33.1	SZH 34.1	SZH 32.1	SZH 32.2	SZH 39.1
Element										
Nd146	80.96	113.32	3.06	21.03	37.02	7.11	8.85	2.86	1.879	1.301
Sm147	37.02	54.77	3.74	12.48	18.13	15.33	18.13	5.74	4.07	3.96
Eu151	2.81	4.49	0.460	1.245	1.878	1.363	2.70	0.866	0.506	0.385
Gd157	85.58	106.44	20.67	31.73	47.61	75.74	81.58	29.97	25.54	26.45
Yb172	975.20	1200.88	774.79	689.59	882.62	905.67	1068.67	560.39	760.75	884.18
Lu175	175.16	150.41	97.48	82.20	122.68	127.09	115.28	63.04	88.27	100.19
Hf179	11193.32	11023.72	12974.07	10345.34	11108.52	8055.80	9412.56	8564.58	9666.96	9921.35
1 σ error										
Element										
Nd146	3.97	5.65	0.17	1.09	1.93	0.32	0.40	0.14	0.094	0.071
Sm147	2.20	3.32	0.25	0.79	1.17	0.78	0.92	0.31	0.22	0.22
Eu151	0.14	0.22	0.028	0.067	0.099	0.062	0.12	0.042	0.026	0.021
Gd157	4.95	6.26	1.25	1.94	2.94	3.79	4.10	1.53	1.31	1.37
Yb172	55.43	69.27	45.36	40.99	53.28	45.18	53.58	28.27	38.64	45.26
Lu175	9.56	8.32	5.46	4.67	7.06	6.20	5.65	3.11	4.38	5.00
Hf179	474.95	467.80	550.51	438.98	471.34	341.83	399.40	363.42	410.18	420.98

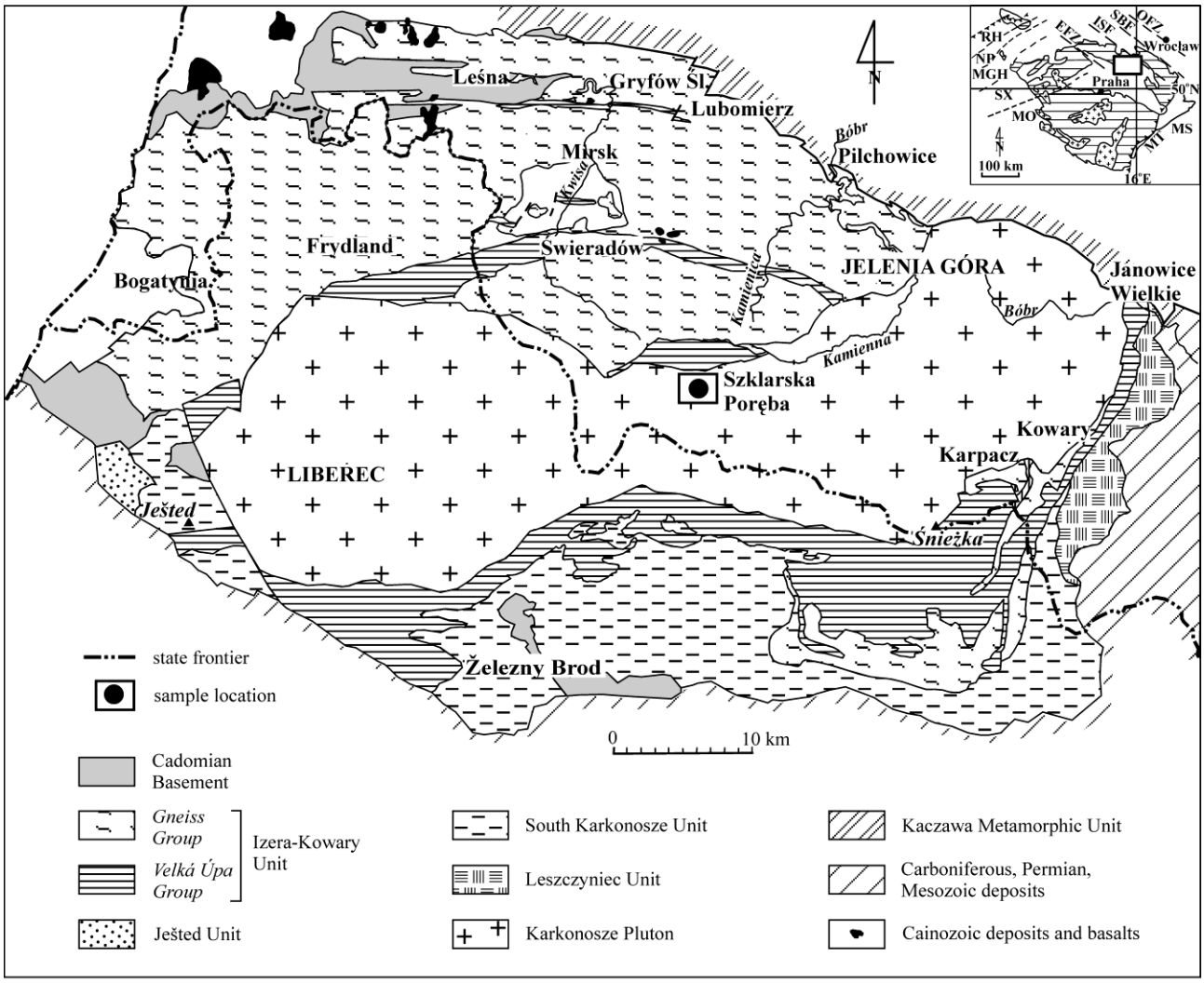

Fig. 1.

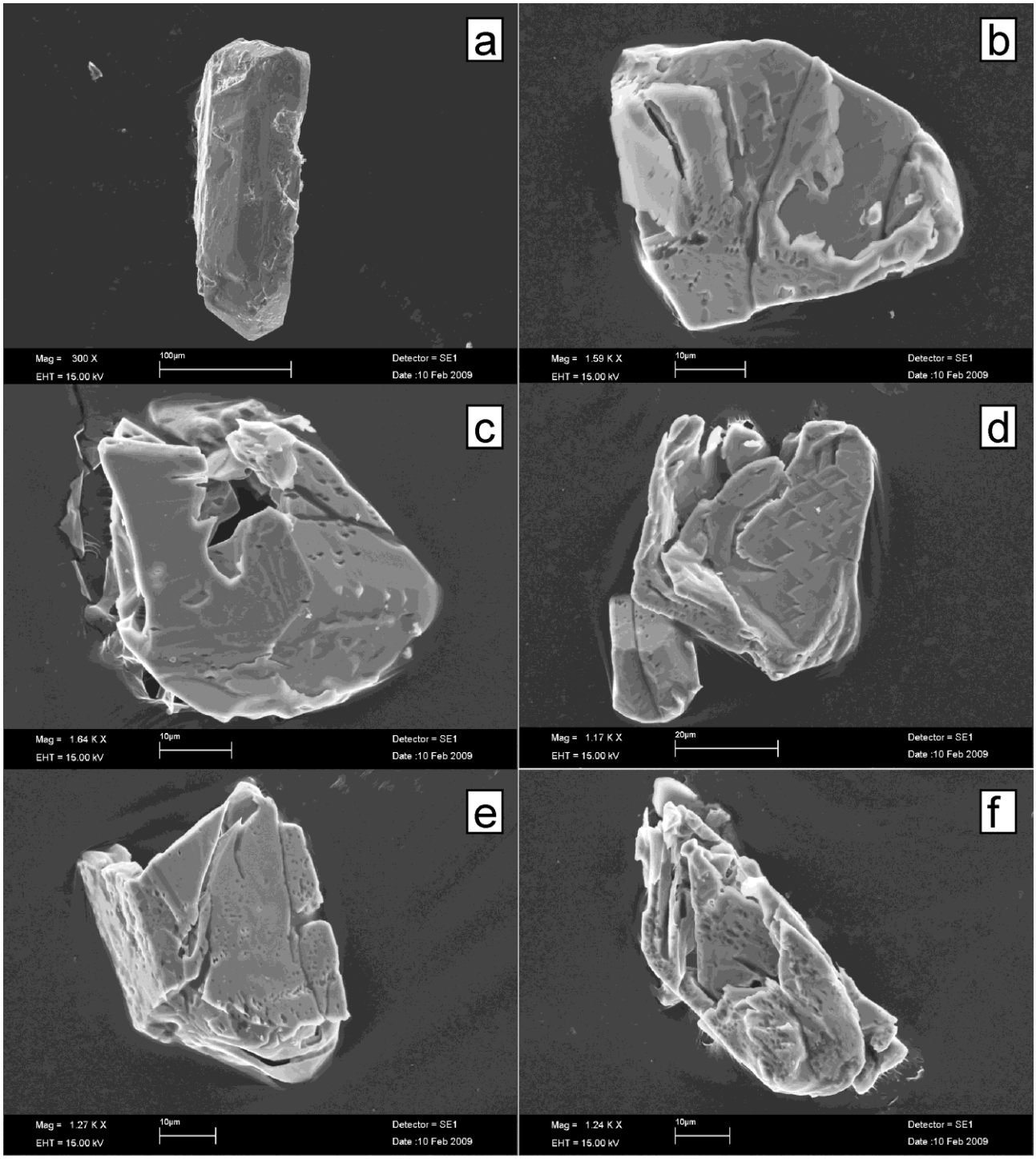

Fig. 2.

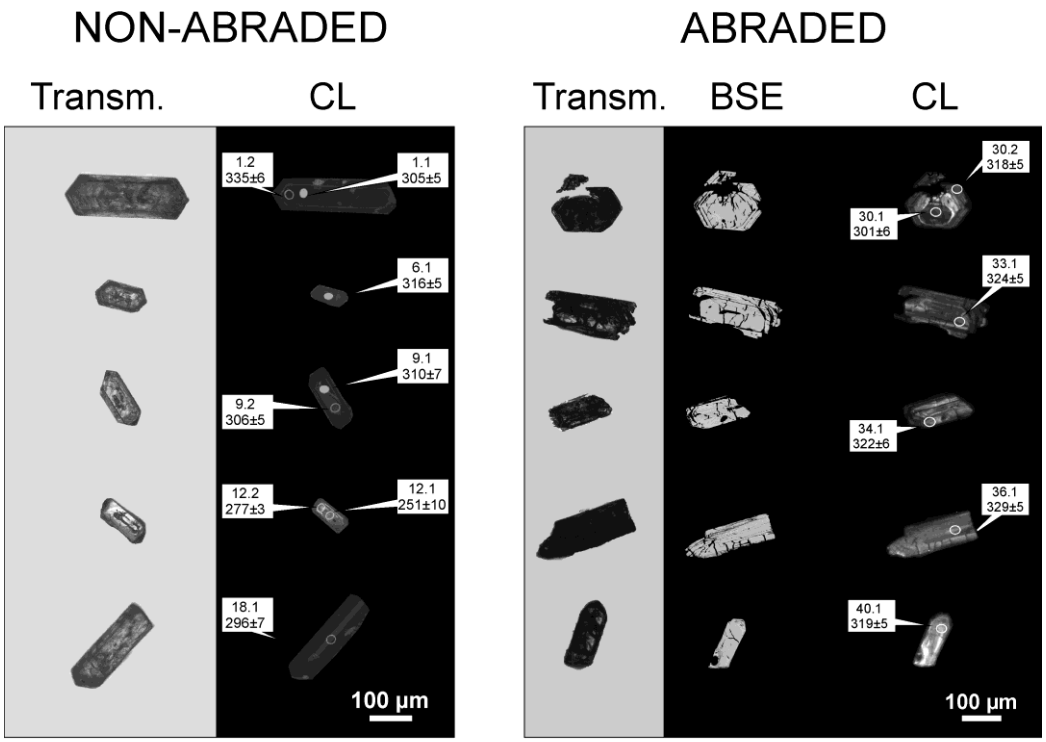

Fig. 3.

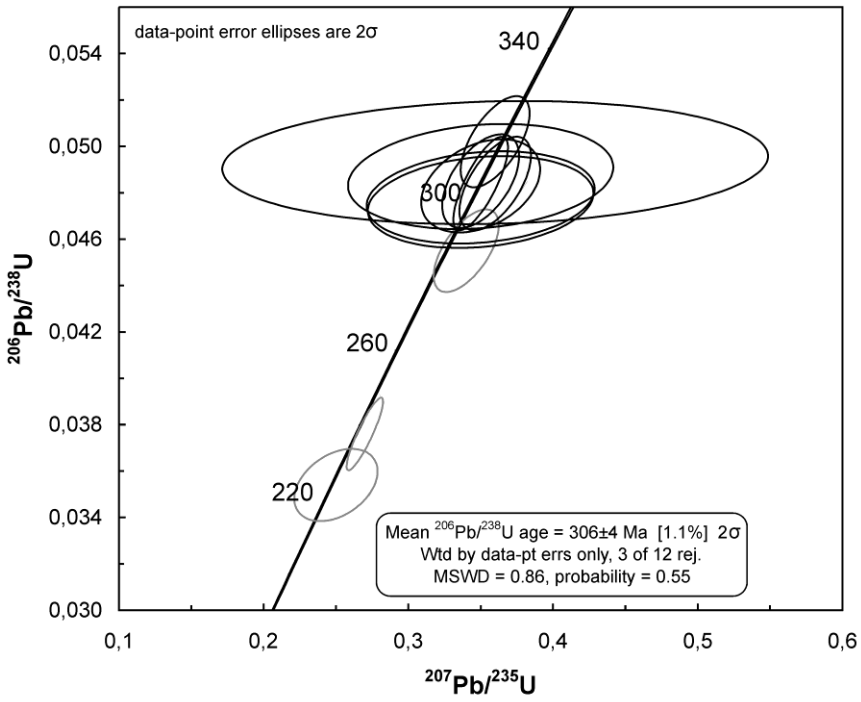

Fig. 4.

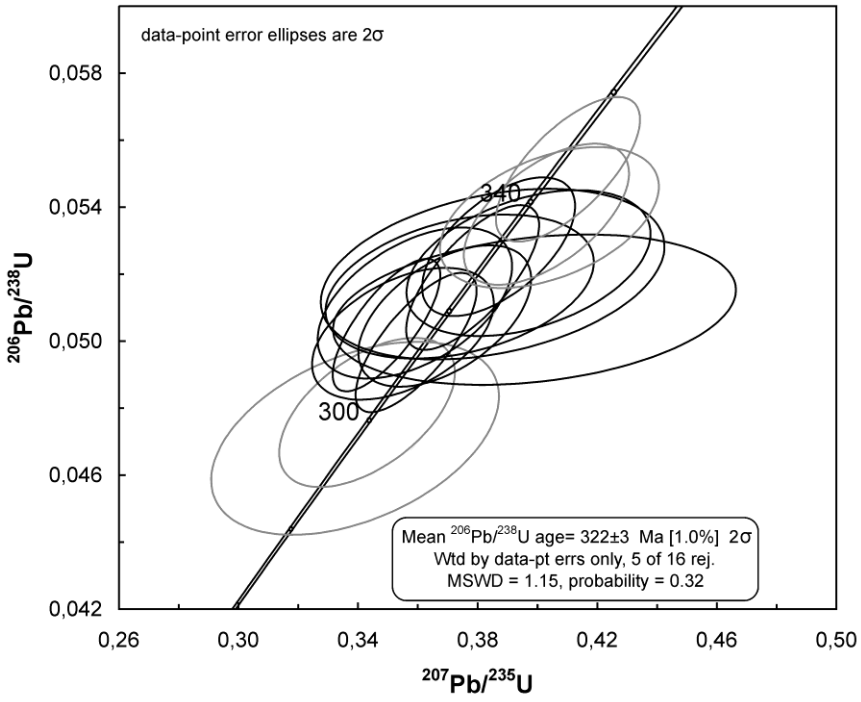

Fig. 5.

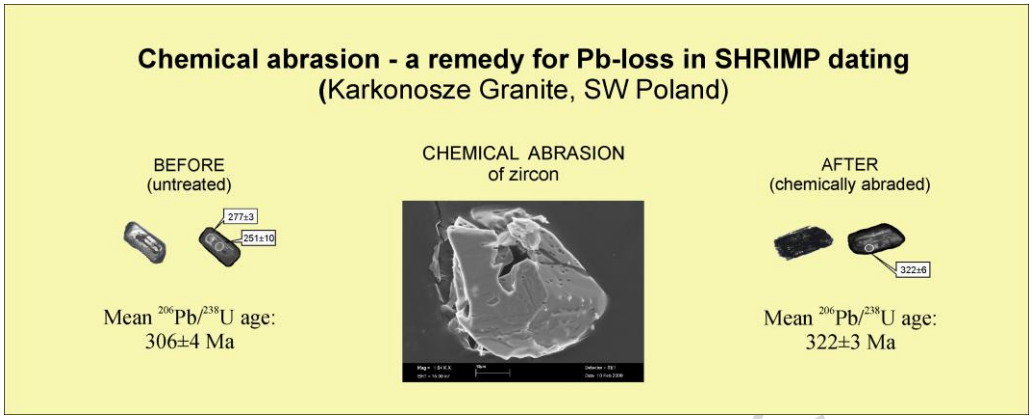

Graphical Abstract

Highlights

A chemical abrasion technique can be applied to U–Pb zircon SHRIMP geochronology.
This is illustrated using U-rich zircons from the Karkonosze Granite, SW Poland.
Untreated zircons give 306±4 Ma while CA zircons give 322±3 Ma ($^{206}Pb/^{238}U$ ages).